THE ASTROPHYSICAL JOURNAL, 495:740–748, 1998 March 10

WATER MASER EMISSION AND THE PARSEC-SCALE JET IN NGC 3079

ADAM S. TROTTER, LINCOLN J. GREENHILL, JAMES M. MORAN, AND MARK J. REID
Harvard-Smithsonian Center for Astrophysics, 60 Garden Street, Cambridge, MA 02138
JUDITH A. IRWIN
Queen's University, Stirling Hall, Room 308E, Kingston, ON K7L 3N6 Canada
AND
KWOK-YUNG LO
University of Illinois, 1002 W. Green Street, Urbana, IL 61801
Received 1997 August 20; accepted 1997 October 16

ABSTRACT

We have conducted VLBI observations at subparsec resolution of water maser and radio continuum emission in the nucleus of the nearby active galaxy NGC 3079. The 22 GHz maser emission arises in compact ($\sim$0.01 pc at a distance of 16 Mpc) clumps, distributed over $\sim$2 pc along an axis that is approximately aligned with the major axis of the galactic disk. The Doppler velocities of the water maser clumps are consistent with their lying in the inner parsec of a molecular disk with a binding mass $\sim 10^6$ $M_\odot$, rotating in the same sense as the edge-on kiloparsec-scale molecular disk observed in CO emission. However, the velocity field has a significant nonrotational component, which may indicate supersonic turbulence in the disk. This distribution is markedly different from that of water masers in NGC 4258, which trace a nearly perfectly Keplerian rotating disk with a binding mass of 3.5×10^7 $M_\odot$. The 22 GHz radio continuum emission in NGC 3079 is dominated by a compact (<0.1 pc) source that is offset 0.5 pc to the west of the brightest maser feature. No bright maser emission is coincident with a detected compact continuum source. This suggests that the large apparent luminosity of the maser is not caused by beamed amplification of high brightness temperature continuum emission. At 8 and 5 GHz, we confirm the presence of two compact continuum sources with a projected separation of 1.5 pc. Both have inverted spectra between 5 and 8 GHz and steep spectra between 8 and 22 GHz. NGC 3079 may be a nearby, low-luminosity example of the class of compact symmetric gigahertz-peaked spectrum radio sources. We detected a third continuum component that lies along the same axis as the other two, strongly suggesting that this galaxy possesses a nuclear jet. Faint maser emission was detected near this axis, which may indicate a second population of masers associated with the jet.

Subject headings: galaxies: active — galaxies: individual (NGC 3079) — galaxies: jets — galaxies: nuclei — masers

1. INTRODUCTION

NGC 3079 is a nearly edge-on ($i = 84°$) SBc galaxy at a distance of 16 Mpc ($H_0 = 75$ km s^{-1} Mpc^{-1}; 1 mas corresponds to 0.08 pc). Kiloparsec-scale radio lobes (Duric & Seaquist 1988) and loops of Hα emission (Ford et al. 1986) extend along the minor axis of the galactic disk. Ionized material in these lobes shows evidence for a $\sim$2000 km s^{-1} outflow (Duric & Seaquist 1988; Filippenko & Sargent 1992; Veilleux et al. 1994). Heckman (1980) classified the optical emission spectrum of NGC 3079 as that of a LINER, which could indicate shock-induced ionization in the galaxy (see, e.g., Dopita 1995). Irwin & Seaquist (1991) fitted three-dimensional galactic disk models to H I line emission and determined a systemic velocity of 1116 ± 1 km s^{-1} with respect to the local standard of rest (LSR) for the radio astronomical definition of velocity, $v/c = -\Delta v/v_0$ (at $v_{\rm sys}$, $v_{\rm LSR,Rad} = v_{\rm Hel,Opt} - 0.9$ km s^{-1}). Observations of CO emission revealed a dense, rotating molecular ring extending $\sim$200 to 750 pc from the nucleus along a position angle of $-15°$ (Young, Claussen, & Scoville 1988; Sofue & Irwin 1992). The disk rotates as a solid body out to a radius of 400 pc, where the velocity is 330 km s^{-1}. Within a 400 pc radius, the disk has a mean molecular density of 530 cm^{-3} and a total molecular mass $M_{\rm H_2} \sim 5 \times 10^9$ $M_\odot$, or about 50% of the dynamical mass in this inner region of the galaxy. Irwin & Sofue (1992) inferred a systemic velocity for the rotating CO disk of 1145 ± 10 km s^{-1}, nearly 40 km s^{-1} greater than the systemic velocity inferred for the galactic disk from H I emission (Irwin & Seaquist 1991); the origin of this discrepancy is unclear.

Large-scale outflows of the type observed in NGC 3079 have been observed in a number of galaxies that exhibit high far-infrared (FIR) luminosities and evidence for starburst activity (see, e.g., Heckman, Armus, & Miley 1990). However, Hawarden et al. (1995) present a number of arguments against the starburst hypothesis in NGC 3079:

1. Despite an unusually large concentration of molecular gas in the inner kiloparsec, the low ratio of FIR luminosity to molecular mass (Young et al. 1988) indicates that the star formation efficiency is not very high.
2. The 10 μm emission does not appear to be centrally concentrated (Devereaux 1987), as would be expected if there were starburst activity in the nucleus.
3. The mid-IR spectral energy distribution is relatively flat, which is atypical of starburst galaxies (Hawarden et al. 1986).
4. The inferred extinction toward the nucleus, $A_V \sim 7.5$ mag, is lower than expected for a dusty starburst region.

An alternative model for the origin of the outflow in NGC 3079 was proposed by Duric & Seaquist (1988), who suggested that a jet from a compact central engine could be directed along the minor axis of the galactic disk by inter-

action with dense gas in the nuclear environment. This interaction should result in strong shocks in the molecular gas in the nucleus. The observed strength of emission in the lower vibrational transitions of H_2 is consistent with collisional excitation in strong ($v \sim 150$ km s^{-1}) shocks (Hawarden et al. 1995). Blueshifted OH maser emission to the south of the nucleus (Baan & Irwin 1995) may mark the boundary between a dense nuclear disk and a nuclear cavity swept clear by outflowing material.

A 5 GHz VLBI observation of the nucleus of NGC 3079, made in 1986 by Irwin & Seaquist (1988; hereafter IS) revealed two compact continuum components, each ≈ 12 mJy and with a projected separation of 1.5 pc along an axis with a position angle 123° east of north. Following the convention of IS, we will refer to the southeastern compact feature as "component A" and to the other as "component B." An extended feature ("component C") lying between A and B was tentatively identified, but its characteristics were not well constrained by the observation. The quoted 5 GHz flux density of the entire nucleus (at subarcsecond resolution) ranges between 60 and 100 mJy (see Hawarden et al. 1995), which implies that components A and B contribute at most 40% of the total nuclear continuum emission at this frequency. IS argued that if the compact VLBI sources are features in a jet confined by the ambient nuclear medium, then the momentum flux in the inner parsec of NGC 3079 is sufficient to power the kiloparsec-scale outflow (see also Duric & Seaquist 1988). Irwin & Sofue (1992) find evidence in CO emission of a component of molecular gas with high velocity dispersion, flowing away from the nucleus along the A-B axis. They suggest that "spurs" in the CO images along a position angle of $\sim 30°$ may indicate a second outflow perpendicular to the one along the A-B axis.

Pedlar et al. (1996) observed that the nuclear H I absorption profile is comprised of a deep feature at 1140 km s^{-1} flanked by redshifted and blueshifted features offset at ± 100 km s^{-1}. Baan & Irwin (1995) observed a similar profile in H I and OH absorption, although they found that the redshifted absorption peaks ~ 20 pc to the south of the other components. VLBI images at 21 cm (Satoh et al. 1998) showed an H I absorption feature at continuum component B that is redshifted by ~ 200 km s^{-1} with respect to a similar feature at component A; absorption at velocities intermediate to these two features is seen at some level against both components.

The nucleus of NGC 3079 is a site of intense H_2O maser emission, the majority of which is distributed over a velocity range of ~ 100 km s^{-1}, centered on $v_{LSR} \approx 1000$ km s^{-1} (Henkel et al. 1984; Haschick & Baan 1985). The flux density of the brightest feature, at 957 km s^{-1}, has varied between 1 and 8 Jy over a 10 yr monitoring period (Baan & Haschick 1996), with ~ 4 Jy variations occurring on timescales of months. The average line width is ~ 5 km s^{-1}. With the exceptions of a 140 mJy feature at $v_{LSR} = 1190$ km s^{-1} (Nakai et al. 1995) and a faint feature at 1123 km s^{-1} (this paper), all of the known H_2O maser emission is blueshifted relative to the systemic velocity. It has been suggested (see, e.g., Haschick et al. 1990; Baan & Irwin 1995) that the extreme brightness of the H_2O maser in NGC 3079 could result from highly beamed, unsaturated amplification of 22 GHz emission from compact sources by foreground molecular gas. A VLBI observation made in 1988 (Greenhill 1990) revealed that the majority of the maser emission is confined to a region ~ 0.2 pc in diameter, distributed among several compact clumps 0.002–0.02 pc in extent. Two clumps with a projected separation of 0.08 pc lie 0.5 pc to the north of this region. Several of the unresolved maser clumps exhibit emission over an unusually broad Doppler velocity range, up to 25 km s^{-1}. Multiple spectral features in the emission from a few of the clumps indicate the presence of unresolved spatial components. Velocity gradients were observed within some of the more extended clumps.

We present new images of the water maser emission and the 5, 8, and 22 GHz continuum emission in the inner parsec of NGC 3079, made with the NRAO[1] Very Long Baseline Array (VLBA). Interpretation of the images is strengthened by the determination of accurate relative positions of the maser and the 22 GHz continuum emission. Section 2 describes our VLBA spectral line and continuum observations. We present images of the water maser emission in § 3 and images of the 5, 8, and 22 GHz continuum emission in § 4. Section 5 discusses the implications of these results for models of the nucleus of NGC 3079. Section 6 summarizes our results.

2. OBSERVATIONS

We observed the 6_{16}–5_{23} transition of H_2O (rest frequency $\nu_0 = 22.23508$ GHz) toward NGC 3079 for 8 hr on 1995 January 9, using the NRAO VLBA and the VLA, which operated as a phased array of 27 antennas. The data were recorded in left circular polarization in four 8 MHz passbands of 512 spectral channels each (0.21 km s^{-1} channel spacing). The band-center LSR velocities were 1150, 1020, 934, and 800 km s^{-1}, with the fourth bandpass tuned to lie outside of the known velocity range of maser emission. The data were processed on the VLBA correlator, and postcorrelation processing was performed with AIPS. Amplitude calibration included estimated corrections for atmospheric opacity and elevation-dependent variations in antenna gain. We calibrated residual delays and fringe rates and complex bandpass response with observations of 3C 273, NRAO 150, and 4C 39.25. We referenced the phases of all spectral channels to a single strong channel (at 954.5 km s^{-1}) on the edge of the brightest maser feature. To image the maser emission, we coherently averaged the visibility data in sets of four spectral channels. To image the continuum, we averaged over all the channels in the bandpass tuned to lie outside the known range of maser emission.

The 5 and 8 GHz continuum observations were made on 1992 September 15 and 29. The 5 GHz observations used an array consisting of the VLBA stations at Hancock, Kitt Peak, and Los Alamos, the NRAO 140 foot (43 m) antenna at Green Bank, and the VLA phased array. The 8 GHz observations were made with a VLBI array consisting of the VLBA stations at Hancock, Fort Davis, and Kitt Peak, the NRAO 140 foot antenna, the 100 m antenna of the MPIR at Effelsberg, and the VLA phased array. The fringe calibrator sources for the continuum observations were OJ 287 and 0917+624. NGC 3079 was observed with a bandwidth of 28 MHz for a total of 2 hr at each frequency. The data were correlated with the MkIII correlator at Haystack Observatory. Postprocessing and synthesis imaging were

[1] NRAO is operated by Associated Universities, Inc., under cooperative agreement with the National Science Foundation.

TABLE 1

PROPERTIES OF NATURALLY WEIGHTED IMAGES

ν (GHz)	Synthesized Beam: Major Axis (mas)	Minor Axis (mas)	P.A. (deg)	1 σ (mJy beam^{-1})
5	8.4	2.5	3	0.11
8	1.8	0.6	−34	0.16
22[a]	1.15	0.98	5	0.22
22[b]	1.15	0.98	5	2.8
22[c]	3.34	2.98	47	0.27

[a] Continuum (100 km s^{-1} average).
[b] Spectral line (0.8 km s^{-1}).
[c] Continuum with 100 Mλ (u, v) taper.

performed in AIPS. Table 1 lists the naturally weighted restoring beam and 1 σ image noise for our observations.

3. WATER MASER EMISSION

Figure 1 (Plate 18) shows the angular and velocity distributions of water maser emission in the nucleus of NGC 3079. Figure 2 is a spectrum generated from the total imaged flux density in each 0.8 km s^{-1} spectral channel. The emission arises in compact ($\lesssim$0.02 pc) "clumps," most of which lie in a 0.2 pc diameter cluster with a velocity range $930 < v_{\rm LSR} < 1060$ km s^{-1}; this cluster includes the maser peak (3.6 Jy at $v_{\rm LSR} = 957$ km s^{-1}), shown at the origin of the map in Figure 1. Two additional clumps 0.5 pc (7 mas) to the north overlap the main cluster in Doppler velocity, emitting over a range $1000 < v_{\rm LSR} < 1040$ km s^{-1}. The overall distribution of the H_2O maser features we observed in 1995 January is similar to that seen in 1988 February (Greenhill 1990), although certain clumps have faded while new ones have appeared. Clumps that appear to be common to both epochs coincide to $<$0.1 mas, although proper motions between two epochs, for spectrally blended features, cannot be estimated reliably. The normalized fringe visibility amplitude of the maser peak is $>$0.9 on our longest baseline (6500 km). We therefore place an upper limit of 20 μas on the angular size of the maser peak (linear size $\lesssim 5 \times 10^{15}$ cm) and a lower limit of $T_B > 3 \times 10^{13}$ K on the peak brightness temperature. Haschick et al. (1990) obtained a similar lower limit on the peak brightness temperature with a four-station intercontinental VLBI observation in 1986 October.

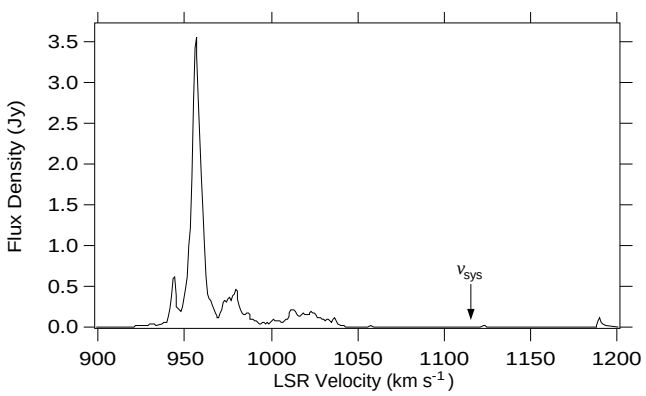

FIG. 2.—Spectrum of total imaged maser flux density. The Doppler velocity spacing of the spectral channels is 0.8 km s^{-1}. The LSR systemic velocity of 1116 km s^{-1} is indicated with an arrow.

Some of the clumps are extended and exhibit apparent gradients in radial velocity. For example, the maser peak, at 957 km s^{-1}, lies in a $\sim$0.02 pc elongated clump (Fig. 1, *inset*) oriented roughly northwest to southeast that exhibits a projected Doppler velocity gradient of nearly 4000 km s^{-1} pc^{-1}. Gradients of similar magnitude are present in other clumps, though their position angles do not appear to be correlated with each other or with any larger scale nuclear structure. If the masers do in fact lie in a nearly edge-on disk, extended clumps are likely to be foreshortened, and so the apparent velocity gradients should be regarded as upper limits. Note that the blending of two or more features that are poorly resolved in angle and velocity can mimic a velocity gradient in an extended structure. Thus, the gradients we observe do not necessarily imply the presence of coherent, rotating structures in the molecular gas. However, in the case of the extended clump containing the maser peak, "kinks" in the structure belie the presence of more than two unresolved subfeatures, and these kinks at least display a true dependence of Doppler velocity on position within the clump, a dependence which cannot be attributed to spectral blending alone.

We detected two redshifted maser features. The first is a single 140 mJy feature 1.2 pc south southeast of the maser peak at a $v_{\rm LSR}$ of 1190 km s^{-1}. This feature was first identified in a single-antenna spectrum from 1995 April (Nakai et al. 1995). Including this redshifted feature with the blueshifted clumps to the north, we find that the maser emission in the nucleus of NGC 3079 extends a projected distance of 1.7 pc along an axis with a position angle of about $-10°$ (Fig. 1). This axis is approximately aligned with the major axis of the kiloparsec-scale galactic disk (position angle = $-15°$) as seen in optical, H I (Irwin & Seaquist 1991), and CO (Young et al. 1988; Sofue & Irwin 1992) images. The second redshifted feature lies off of this north-south axis, 1.2 pc southeast of the 22 GHz continuum peak (§ 4), at a $v_{\rm LSR}$ of 1123 km s^{-1}. This feature is angularly coincident with a faint, extended 22 GHz continuum source. We note that a second maser feature, at 1040 km s^{-1}, also lies off the north-south axis, 0.2 pc northwest of the 22 GHz continuum peak. These off-axis features define a second axis, with a position angle of 128°, that is shared by the nuclear continuum components. This suggests that there is a second population of water masers in NGC 3079 that may be interacting with or amplifying the jet.

4. THE PARSEC-SCALE RADIO CONTINUUM

Figures 3, 4, and 5 show naturally weighted 5, 8, and 22 GHz images of the parsec-scale continuum emission in the nucleus of NGC 3079. Table 2 lists the fitted parameters of the compact continuum sources identified at each of these frequencies. Figure 6 compares the flux densities of the two brightest continuum components, A and B.

4.1. 5 GHz *Continuum*

At 5 GHz, we detected both continuum components A and B of IS. The angular separation of the peaks of these two components is within 1.4 mas of that measured in 1986 February, from which we place an upper limit on the relative proper motion of the two continuum features of 200 μas yr^{-1} (0.06c). Because of the limited (u, v) coverage of the 5 GHz VLBI observation, no substructure was resolved in either component. Note that while the flux density of B in 1992 is approximately the same as that measured by IS in

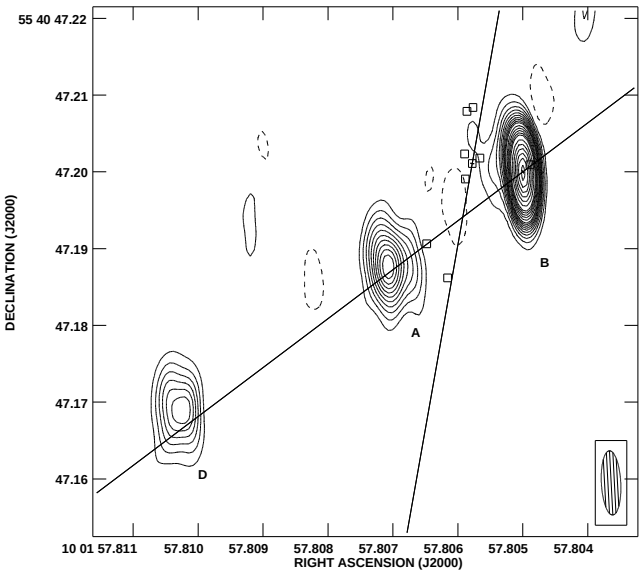

FIG. 3.—Naturally weighted, self-calibrated image of the 5 GHz nuclear continuum, from a VLBI observation from 1992 September. Image contours are -1, 1, 2, 3, 4, 5, 6, 7, 8, 9, 10, 12, 14, 16, 18, 20, 25, 30, 35, 40, 45, and 50×0.3 mJy beam^{-1} ($1\ \sigma = 0.11$ mJy beam^{-1}). Emission peak is at 16 mJy beam^{-1} (component B). The axis of the maser feature distribution and the axis of the nuclear jet are indicated by solid lines. Boxes mark the positions of selected maser features.

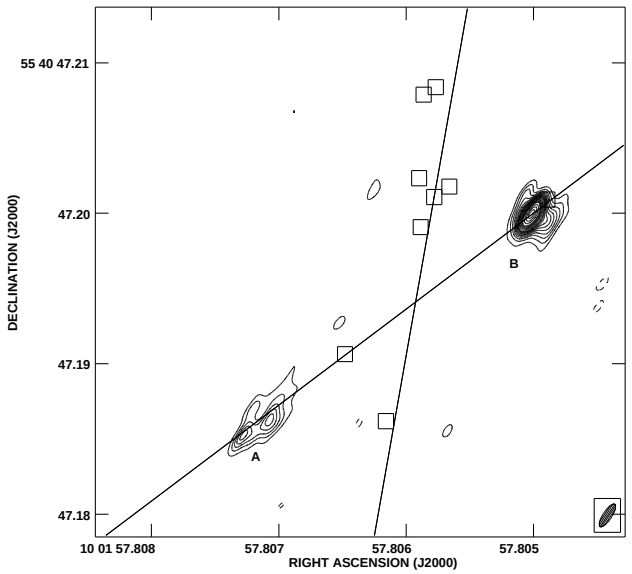

FIG. 4.—Naturally weighted, self-calibrated image of 8 the GHz nuclear continuum, From a VLBI observation from 1992 September. Image contours are at -1, 1, 2, 3, 4, 5, 6, 7, 8, 9, 12, 14, 16, 18, 20, 25, and 30×0.5 mJy beam^{-1} ($1\ \sigma = 0.16$ mJy beam^{-1}). The axis of the H_2O maser emission and the axis of the nuclear jet are indicated by solid lines. Boxes indicate positions of selected maser features.

1986, component A appears to have faded somewhat (Table 2). However, given the quoted uncertainties in the flux density measurements of IS, it is not possible to determine with this observation whether either component is in fact variable at 5 GHz. We did not detect the extended continuum component C reported by IS. However, component A exhibits an extension to the west at the 15 σ level (Fig. 3), and there is some indication of emission that is undersampled by our shortest baselines.

We report the detection of a third continuum component (labeled D in Fig. 3 and Table 2), located $\sim$4 pc southeast of B along the A-B axis. Component D is not visible at the 0.5 and 0.7 mJy beam^{-1} (3 σ) level at 8 and 22 GHz, respectively. Given the deconvolved size of this source at 5 GHz, $\sim 4 \times 3$ mas, it would be significantly resolved at 8 and 22 GHz (see Table 1). Experimentation with various subsets of the visibility data indicates that component D could have a flat spectrum and still be undetectable in our higher frequency images. However, we can rule out a rising spectrum above 5 GHz. This differs from A and B, both of which clearly peak between 5 and 22 GHz (Table 2).

4.2. 8 GHz *Continuum*

At 8 GHz we also detected both continuum components A and B. Component B is comparatively strong and extends $\sim$0.1 pc along a position angle of 60°. Component A is

TABLE 2

NUCLEAR CONTINUUM COMPONENTS IN NGC 3079

Feature	r (mas)	ϕ (deg)	Major Axis (mas)	Axis Ratio	P.A. (deg)	S_0 (mJy)
22 GHz (1995 January)						
B.....	...	...	1.2 ± 0.1	1.3 ± 0.2	170 ± 10	16 ± 1
A	24.1 ± 0.3	127 ± 2	$\lesssim 3$	...	...	6 ± 1
C	15.4 ± 0.5	126 ± 2	7.4 ± 0.6	2.2 ± 0.5	90 ± 10	11 ± 2
8 GHz (1992 September)[a]						
B.....	...	...	1.3 ± 0.1	1.4 ± 0.2	57 ± 4	37 ± 2
A	22.7 ± 0.3	127.7 ± 0.7	4.0 ± 0.4	3 ± 1	134 ± 5	15 ± 2
5 GHz (1992 September)						
B.....	...	...	<2.3	...	...	16.8 ± 0.4
A	21.3 ± 0.2	124.9 ± 0.6	<4.5	...	...	6.0 ± 0.5
D	54.5 ± 0.4	124.7 ± 0.4	4 ± 1	~ 1	...	4.3 ± 0.5
5 GHz (1986 June; Irwin & Seaquist 1988)						
B.....	...	...	<3	...	...	12 ± 7
A	20.2 ± 0.3	122.6 ± 0.3	<3	...	...	12 ± 5
C	17 ± 5	130 ± 50	<20	...	...	<45

[a] Image convolved to a resolution of 2 mas to smooth out substructure.

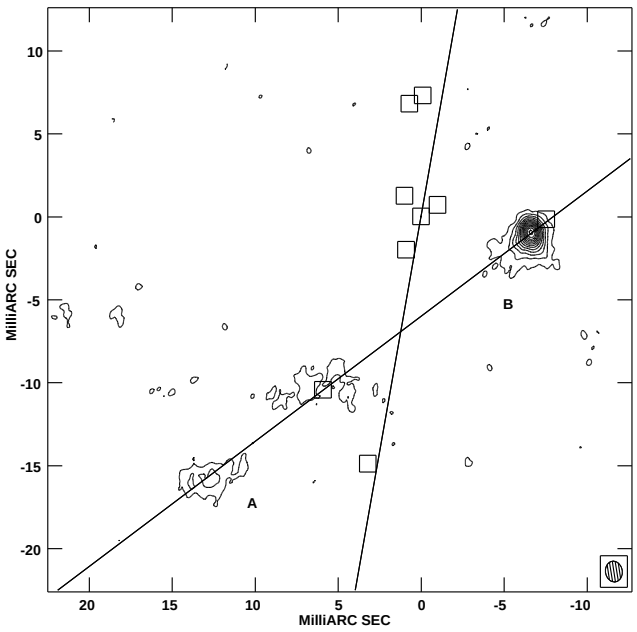

FIG. 5a

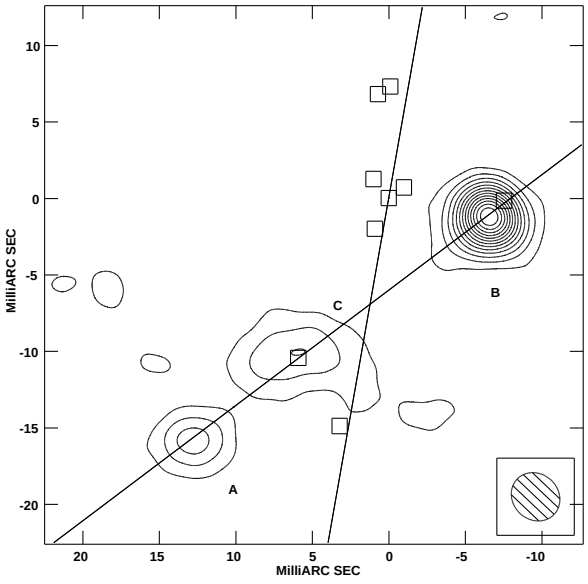

FIG. 5b

FIG. 5.—(*a*) Naturally weighted 22 GHz continuum image created by phase-referencing spectral visibilities to the maser peak and coherently averaging over a velocity range of $750 < v < 850$ km s^{-1}. The contours are in units of 0.7 mJy beam^{-1} (1 σ = 0.22 mJy beam^{-1}). Solid lines indicate the axis of the H_2O maser distribution and the axis of the nuclear jet. Boxes indicate the positions of selected maser features. (*b*) Same as in (*a*), but with a 100 Mλ taper applied to the (*u*, *v*) data before imaging. Image contours are in units of 1 mJy beam^{-1} (1 σ = 0.27 mJy beam^{-1}).

clearly composed of multiple features, clustered within $\sim$0.2 pc of each other. The measured flux densities of these subcomponents range from 2 to 7 mJy, and their angular sizes are typically $\lesssim$2 mas (0.15 pc). Relative to B, the centroid position of component A is $\sim$2 mas to the southeast (along a position angle of 160°) of that observed at 5 GHz. This difference is likely caused by differences in the brightness distribution within A at the two frequencies; the 8 GHz substructure appears to trace the limb-brightened southeast edge of an extended source that is centered near the 5 GHz position. The integrated flux densities of both A and B are

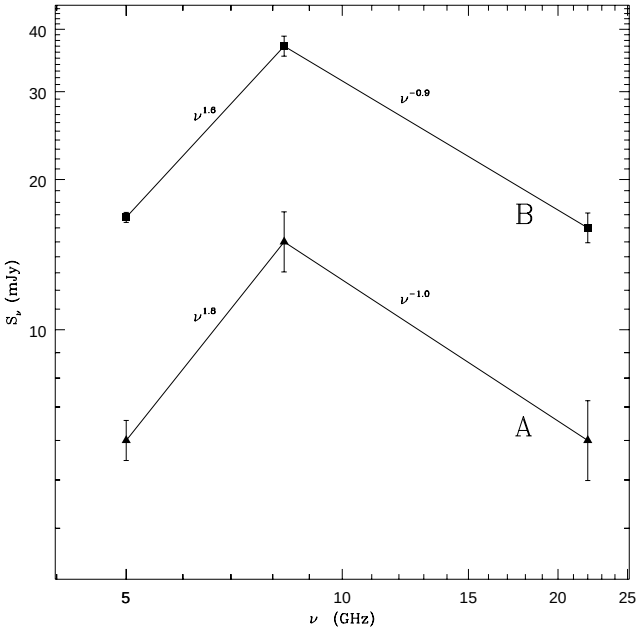

FIG. 6.—Spectra of the compact continuum components A and B at 5, 8, and 22 GHz. The spectral indices of both components between 5 and 8 GHz and between 8 and 22 GHz are indicated.

greater at 8 GHz than at 5 GHz. Assuming they did not vary significantly in flux over the 12 days separating the observations, we find that both sources have inverted spectra between 5 and 8 GHz: $\alpha_A = -1.8$, and $\alpha_B = -1.6$.

4.3. 22 GHz *Continuum*

We imaged both continuum components A and B at 22 GHz (Fig. 5) by phase-referencing the spectral visibilities to the maser peak and averaging over an apparently line-free velocity range of $750 < v_{LSR} < 850$ km s^{-1}. The maser peak lies 6.7 $\pm$ 0.1 mas to the east-northeast of component B, at a position angle of 81°. We detect no 22 GHz continuum emission to a 3 σ limit of 0.75 mJy beam^{-1} at the position of any of the maser features in the north-south distribution described in § 3. The 22 GHz emission is dominated by component B with an integrated flux density of $\sim$16 mJy. Figure 5*b* was produced with a 100 Mλ Gaussian taper applied to the visibility weights in the (*u*, *v*) plane, in order to lower the angular resolution and thus reveal more extended emission. Inspection of the images reveals that B consists of a $\sim$10 mJy unresolved core plus a $\sim$6 mJy halo extending $\sim$0.1 pc to the south-southeast. Fainter halo emission is visible in the untapered image at the 6 σ ($\lesssim$2 mJy beam^{-1}) level, extending $\sim$0.2 pc to the southeast along the jet axis (Fig. 5a). The integrated flux density of B at 22 GHz in 1995 January is clearly less than it was at 8 GHz in 1992 September (Fig. 6); if the component is not intrinsically variable, we find a spectral index $\alpha_B = 0.9$ between these two frequencies. However, the fitted size of this component at both frequencies is $\lesssim$0.1 pc, so flux variations on timescales of years would not violate light-travel time constraints.

In the high-resolution 22 GHz image (Fig. 5*a*), continuum component A has a poorly defined morphology; it peaks at approximately the same position relative to component B as does the easternmost compact subcomponent observed at 8 GHz (Fig. 4). Faint emission at the 3 σ level extends 3 mas around the peak. In the lower resolution tapered image

(Fig. 5*b*), component A has an integrated flux density of ~ 6 mJy, suggesting that it may have a steep spectrum between 8 and 22 GHz, $\alpha_A \approx 1.0$. It is also possible that one or more of the compact subcomponents of A is variable.

The low-resolution 22 GHz continuum image reveals an extended feature, which we label "C," between components A and B. The centroid position of C coincides within measurement errors to the position of component C seen by IS at 5 GHz. It is clearly elongated east to west over ~ 7 mas (0.5 pc). In the higher resolution 22 GHz continuum image (Fig. 5*a*), this source appears mottled at the 3 σ level. Images of intermediate angular resolution suggest that it consists of several compact components distributed along an east-west axis. We did not detect any emission between A and B in our 5 or 8 GHz images. If C consists of multiple compact continuum sources, they must have inverted spectra between 8 and 22 GHz. Alternatively, it may be comprised of multiple, faint maser features distributed between 750 and 800 km s^{-1}. Note that the maser feature at $v_{LSR} = 1123$ km s^{-1} is coincident with the centroid of component C (Fig. 1).

5. DISCUSSION

5.1. *Compact Continuum Sources*

The detection at 5 GHz of three compact continuum features, separated from each other by at least several parsecs and lying along a common axis, strongly suggests that these sample a jet rather than physically unconnected regions of starburst activity. The question then arises as to which component (if any) represents the central engine. Baan & Irwin (1995) suggest that component A is the core and that B is part of the jet, based on the presence of H I and OH absorption features at two distinct velocities in the nucleus. (The angular separation of A and B is unresolved in their images.) If the absorption is caused by material in a disk that rotates in the same sense as the galaxy, the more blueshifted absorption component should be associated with continuum component B, and that near the systemic velocity with component A, which they identify as the core. However, recent high-resolution VLBI observations of H I absorption (Satoh et al. 1998) indicate that the absorption profile toward continuum component B is redshifted with respect to that toward component A. It is not clear whether the absorption profile reflects rotation, outflow, or more complicated motion in the absorbing gas, or whether it is intrinsic to the compact sources.

Typically, the core component of a VLBI core-jet structure in a radio galaxy is compact and has a flat spectrum. In NGC 3079, continuum sources A and B both exhibit extended or multicomponent structure. This is most apparent in the 8 GHz image (Fig. 4), where the morphology of A suggests a jet lobe limb brightened on its leading edge, while B exhibits an extension perpendicular to the jet axis. Also, at 22 GHz (Fig. 5), B appears to consist of an unresolved core containing 75% of the total flux, plus a halo that extends to the south and east. Furthermore, neither component has a flat spectrum (Fig. 6), but, rather, each exhibits a turnover between 5 and 22 GHz suggestive of free-free or synchrotron self-absorption.

The spectra of both sources are quite similar, except that the flux density of A is consistently lower than that of B. If one were a jet component and the other a compact core, we might expect less similarity in their spectra. The nucleus of NGC 3079 may be a low-luminosity, nearby example of the class of compact symmetric objects (CSOs) that exhibit gigahertz-peaked spectra (Phillips & Mutel 1982; O'Dea, Baum, & Stanghellini 1991). These sources have been attributed to bipolar jets from AGNs that are impeded by unusually high-density nuclear gas. In the context of this model, the compact continuum components mark the ram pressure–confined leading edges of a jet that is burrowing out through the dense medium (Readhead et al. 1996). The peaked continuum spectrum may be caused either by synchrotron self-absorption or by free-free absorption in ambient ionized nuclear gas.

It is likely that neither component A nor component B marks the central engine of NGC 3079. If the maser features trace an edge-on disk that feeds the jet (§ 5.2), the core should lie near the intersection of the axes of the maser and continuum distributions. Note also that A and B are roughly equidistant from this point, as would be expected for oppositely directed lobes of a nonrelativistic jet. We therefore suggest that the central engine lies near the midpoint between continuum components A and B.

Component D was detected only at 5 GHz. Nondetection at 8 GHz may be caused in part by resolution effects. However, an inverted spectrum like that of A and B can be ruled out. Since it is nearly twice as far from the assumed position of the central engine, component D may have significantly different physical characteristics from the other two. For example, synchrotron losses may have altered the relativistic electron energy distribution, or the source could have expanded as it traveled farther along the jet. If these three sources are synchrotron self-absorbed emission, the spectrum of D may turn over at a lower frequency than that of A or B. If extrinsic (e.g., free-free) absorption is also occurring, the different spectral characteristics may be a function of different lines of sight through foreground material.

Component C, observed in the low-resolution 22 GHz image (Fig. 5*b*), is close to, but not coincident with, the assumed position of the central engine. Its position also agrees within the measurement errors with the position of continuum component C of IS; however, that source was observed at 5 GHz and was considerably larger (Table 2), so it is not clear that they are the same. Component C is unusual in that it was only detected at 22 GHz, which suggests an inverted spectrum extending to high frequencies. It is possible that C is spectral in nature. A cluster of faint, blueshifted maser features distributed over ~ 100 km s^{-1} in Doppler velocity would appear as a continuum source in the 22 GHz images, which were produced by averaging in frequency over an apparently line-free region of the spectrum (§ 2). This hypothetical maser could amplify an undetected background continuum source in the vicinity of the central engine.

5.2. *The Nature of the Maser Emission*

The sense of rotation of the galactic disk of NGC 3079 is such that the northern side is approaching and the southern side is receding. (The galaxy's inclination of 84° causes the near side of the disk to be projected to the west of the major axis.) The overall distribution of maser Doppler velocities is roughly consistent with their arising in the inner parsec of an edge-on molecular disk that is rotating in the same sense as the kiloparsec-scale molecular disk observed in CO emission (Fig. 7). The center of rotation would be approximately

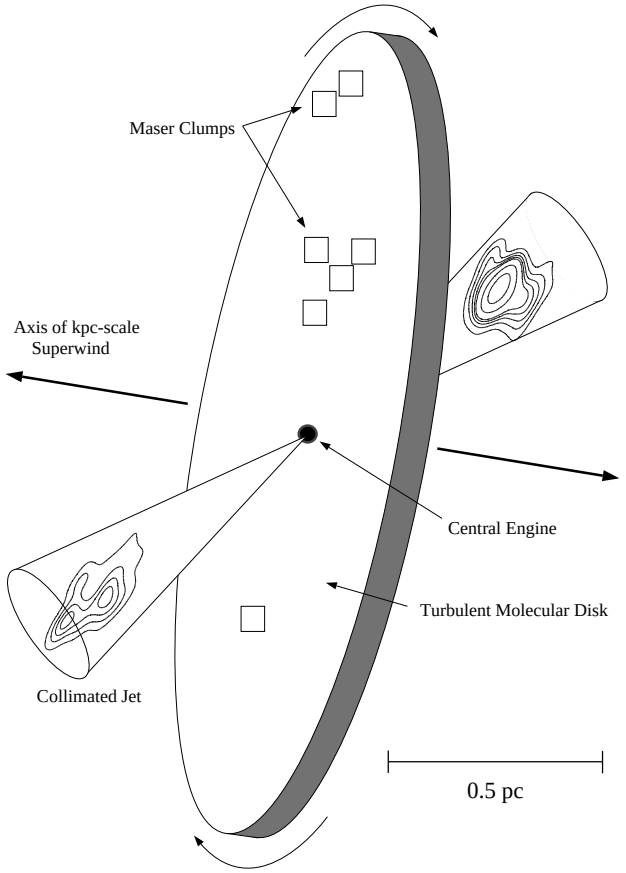

FIG. 7.—Model for the nuclear region of NGC 3079. Here, the maser emission arises in a nearly edge-on disk that is aligned with and rotates in the same sense as the kiloparsec-scale disk seen in CO emission (Sofue & Irwin 1992). Contours show the 8 GHz continuum emission (Fig. 4), and squares indicate the positions of the brighter maser clumps. The pair of cones illustrate the approximate opening angle of the jet; note that the inclination of the jet to the line of sight has not been determined. The central engine is assumed to lie near where the major axis of the maser distribution and the axis of the jet intersect. The disk likely extends to a larger radius than is shown in the schematic illustration, and its thickness is unknown. Arrows indicate the direction of the kiloparsec-scale outflow or "superwind" observed to extend along the minor axis of the galaxy. Note that the jet is misaligned with the axis of the superwind.

midway between the main blueshifted maser cluster and the 1190 km s^{-1} feature to its south. Note, however, that the velocity dispersion of the clumps in the northern (blueshifted) half of this maser structure is comparable to the apparent rotation velocity, $\Delta v \sim v_{\rm rot} \sim 100$ km s^{-1}. Given that the masers do not trace a clear rotation curve, it is difficult to estimate the mass distribution of the inner parsec of NGC 3079. However, the overall velocity distribution is consistent with the presence of a binding mass of $\sim 10^6\ M_\odot$ within 0.5 pc of the center of the putative disk. This system is significantly less well defined than that in the center of NGC 4258, where water masers trace a thin, moderately warped Keplerian disk of inner radius 0.13 pc, outer radius 0.26 pc, and central mass $3.5 \times 10^7\ M_\odot$ (Miyoshi et al. 1995; Herrnstein 1997).

If the masers in NGC 3079 emit isotropically, the total luminosity in the 22 GHz transition is $\sim 200\ L_\odot$ in a volume $\lesssim 0.01$ pc^3. (For comparison, the brightest Galactic water maser source, W49N, has an isotropic luminosity of only $\sim 1\ L_\odot$ in a comparable volume.) It is difficult to account for such a high luminosity with standard maser pumping models (Reid & Moran 1988; Elitzur 1992). However, the true luminosity is probably less than the isotropic luminosity by a factor $\Omega_b/4\pi$, where Ω_b is solid angle into which the maser emission is beamed. Maser amplification of radiation from a compact background source naturally results in small Ω_b. Earlier VLBI and VLA observations established that the centroid of the masing region in NGC 3079 was within 5 mas of the centroid of the nuclear radio continuum source (Haschick et al. 1990). It was predicted that at higher resolution, individual bright water maser features would be seen projected against one or both of the compact continuum components identified in the 5 GHz VLBI image of IS. We have found, however, that no bright maser emission in this galaxy is angularly coincident with any detectable compact continuum emission. The main cluster of maser features is offset by ≈ 5 mas (0.4 pc) from the 22 GHz compact continuum peak (source B).

Highly beamed emission is probably still occurring in NGC 3079. First, the maser features may amplify compact continuum sources that are below our detection threshold, although the observed distribution of maser features would require a complex continuum morphology. Second, superposition of two or more maser features with similar radial velocities along the line of sight can result in highly beamed emission (Deguchi & Watson 1989), although this model may have difficulty reproducing the observed velocity range of bright maser features and the extended structures with velocity gradients. Third, beaming may result from exceptionally high aspect ratios in the molecular gas. For a saturated, velocity-coherent cylinder with a (length/diameter) aspect ratio a, $\Omega_b \approx 1/a^2$ (Goldreich & Keeley 1972; Elitzur, McKee, & Hollenbach 1991).

One model for the pumping of water masers in AGNs relies on irradiation of molecular gas by X-rays from the central engine (Neufeld, Maloney, & Conger 1994). A dense cloud that is illuminated by an external X-ray source will develop a warm layer in which the water abundance is enhanced and in which collisional pumping maintains a population inversion. The presence of dust can greatly increase the depth of this layer by absorbing the infrared photons produced in the pumping process that would otherwise thermalize the molecular energy levels and quench the maser (Collison & Watson 1995; Wallin & Watson 1997). However, the luminosity of the nucleus of NGC 3079 in soft (0.5–3 keV) X-rays is $\sim 1 \times 10^{40}$ ergs s^{-1} (Fabbiano, Feigelson, & Zamorani 1982), and there is no convincing evidence of a nuclear hard X-ray source, obscured or otherwise, from *ASCA* observations (K. Weaver 1997, private communication). Hence, X-ray heating is probably not a significant source of pumping for the water maser in this galaxy.

An alternative pumping model invokes molecular shocks. A fast (~ 100 km s^{-1}) dissociative shock propagating through a medium with a preshock density of $\sim 10^7$ cm^{-3} will leave in its wake a large column of warm (~ 400 K) molecular gas in which the H_2O abundance is enhanced and collisional excitation maintains the maser population inversion (Elitzur, Hollenbach, & McKee 1989, 1992). The resulting sheetlike masing region, when viewed edge-on, provides the long amplification pathlengths and the beaming geometry necessary to produce high brightness temperature maser features. Slower, nondissociative C-type shocks may also produce conditions conducive to water maser emission (Kaufman & Neufeld 1996) and may be

necessary to explain the observed strength of higher energy level water maser transitions in star-forming regions in our Galaxy (see, e.g., Melnick et al. 1993). The detection of strong H_2 emission (Hawarden et al. 1995), high-velocity outflows (see, e.g., Filippenko & Sargent 1992), and dense molecular gas (Young et al. 1988; Sofue & Irwin 1992) all suggest that molecular shocks are present in the nucleus of NGC 3079.

How might shocks be driven in NGC 3079? We suggest a model in which the masers lie in the inner parsec of a dense molecular disk that is shocked by interaction with a loosely collimated nuclear wind. If we assume that the orientation of the inner parsec of the molecular disk in NGC 3079 is the same as observed on larger scales, i.e., nearly edge-on with a position angle of $\sim -15°$ (Sofue & Irwin 1992), then it is clear that the nuclear jet, traced by the compact continuum sources, is not perpendicular to the disk. We suggest that the jet is surrounded by a loosely collimated outflow or "sheath" that disturbs regions of the disk lying under the jet, driving turbulence and shocks that give rise to maser emission. Centrifugally driven outflows from the innermost regions of magnetized accretion disks may be a common feature in AGNs (see, e.g., Königl & Kartje 1994) and could be a source of the hypothesized jet sheath. Note that an outflow originating in the inner accretion disk will not remain axisymmetric about the jet axis but will be redirected along the minor axis of the galaxy, since motion in the plane of the dense molecular disk will be impeded. The redirected outflow will then feed into the kiloparsec-scale radio lobes observed to extend along the minor axis of NGC 3079 (see, e.g., Duric & Seaquist 1988; Veilleux et al. 1994). While certainly not the only conceivable interpretation, this model has the attractive quality of reducing the complexity of the nucleus of NGC 3079 to two relatively simple entities, a dense molecular disk and a misaligned jet with an associated sheathlike outflow.

Irwin & Sofue (1992) detected a kinematic component of CO gas that is distinct from the rotating molecular disk, extending along the jet axis defined by the compact radio continuum sources. (Note that this component accounts for the apparent warp in the disk reported by Sofue & Irwin 1992.) This indicates that molecular gas is somehow being entrained by the jet outflow. The emission we observe at 1123 and 1040 km s^{-1} along the jet axis (Fig. 1) suggests that the entrainment may begin within 1 pc of the central engine, where the gas density is highest. Other galaxies exhibit similar characteristics. Broad linewidth water maser emission is observed extending along the axis of a jet in the LINER NGC 1052 (Diamond et al. 1998), while, in NGC 1068, maser emission marks the deflection of the nuclear jet by a molecular cloud (Gallimore et al. 1996). Thus it appears that the interaction of jets with ambient molecular gas is responsible for at least some of the water maser emission seen in certain AGNs. The presence of water maser emission along the inner parsec of the jet in NGC 3079 lends further credence to the hypothesis that this jet is interacting with the ambient molecular material quite close to the central engine and may be responsible for exciting the brighter emission presumed to lie in the disk itself.

An AGN's disk wind will be ionized, and so lines of sight passing through the outflow will suffer free-free absorption. If the molecular disk is inclined so that the western side is the closer, the orientation of the jet is such that maser emission from the northern, blueshifted side of the disk will not be absorbed. The redshifted emission on the south side, however, will have to traverse the ionized sheath and may be heavily absorbed. This could explain the asymmetry between the blueshifted and redshifted emission in NGC 3079. The presence of multiple continuum jet components may indicate that the outflow occurs in intermittent bursts; the separation of blueshifted maser emission into two distinct clusters may be an effect of two distinct "gusts" of wind from the inner accretion disk. We note, however, that no continuum source analogous to component D was detected to the northwest of component B and that the multiple features may trace standing shocks in the jet rather than intermittent outflow.

Although the relative distribution of redshifted and blueshifted maser emissions in NGC 3079 is consistent with their lying in a roughly edge-on rotating disk, the rotation curve is masked by the large peculiar velocities of individual features. Most notably, the large spread in Doppler velocity ($\Delta v \sim 100$ km s^{-1}) of features in the main cluster containing the maser peak suggests that they are embedded in a region of supersonic turbulence. Such a situation has also been observed in the Galactic star-forming region W49N, where measurement of proper motions of water maser spots has allowed the determination of their true three-dimensional spatial velocities (Gwinn, Moran, & Reid 1992). Statistical analysis of these velocities and the angular distribution of these spots indicates that they are embedded in supersonic turbulence, which may be caused by fluid instabilities in the boundary layer between the ambient medium and a bipolar outflow driven by a young stellar jet (Gwinn 1994; Mac Low et al. 1994). A similar situation may be occurring in NGC 3079. Instabilities in the boundary layer between a nuclear wind and the disk could result in supersonic turbulence. Dense clouds embedded in this turbulence could then collide, producing shocks and maser features over a wide range of radial velocities (Tarter & Welch 1986).

Several authors have considered the acceleration of dense maser clouds by a high-velocity, low-density wind (see, e.g., Strel'nitskii & Sunyaev 1973; Norman & Silk 1979; Elmegreen & Morris 1979). Rescaling the wind-model predictions of Duric & Seaquist (1988) for our adopted distance of 16 Mpc, we estimate a mass-loss rate for the wind of approximately 8 $M_\odot$ yr^{-1} and an outflow velocity of about 5000 km s^{-1}. Taking a typical maser cloud to have a diameter of 0.02 pc (a typical clump size in NGC 3079), a molecular hydrogen number density of 10^9 cm^{-3}, and a distance from the nucleus of 0.5 pc, the ram pressure from this wind is capable of accelerating the cloud to a velocity of 50 km s^{-1} over a distance of 0.05 pc on a timescale of $\sim$2000 yr. However, it is not clear that clouds that are not gravitationally bound can survive being accelerated in this fashion (see, e.g., Hartquist & Dyson 1987, and references therein). It has been proposed that the masers in some AGNs could arise in clouds lifted off the surface of an accretion disk by a centrifugally driven wind (Königl & Kartje 1994; Kartje, Königl, & Elitzur 1996). Magnetic pressure gradients (the so-called "melon seed" force) and radiation pressure on embedded dust are other possible acceleration mechanisms. Alternatively, the clouds could form in the outflow itself via hydrodynamical instabilities, eliminating the need for an acceleration mechanism. A shell driven into the ambient medium can fragment into dense clumps via Rayleigh-Taylor and thermal instabilities (Hartquist & Dyson 1987; Wardle 1990).

6. SUMMARY

We have found no evidence that the unusually bright H_2O maser emission in NGC 3079 is beamed amplification of high brightness temperature 22 GHz continuum emission; the 22 GHz continuum peak lies 0.4 pc east of the maser peak in projection. Both continuum components A and B appear to have inverted spectra between 5 and 8 GHz and, assuming no intrinsic variability, spectral turnovers between 8 and 22 GHz. These spectra may indicate synchrotron self-absorption or free-free absorption in ionized ambient nuclear gas. This source may be a low-luminosity, nearby example of the class of compact, symmetric, gigahertz-peaked spectrum radio galaxies.

Component A shows substructure at 8 GHz that is suggestive of a jet lobe. Component B is somewhat more compact but also exhibits structure at 8 and 22 GHz. A third continuum component (D) was identified at 5 GHz; it lies 4 pc southeast of B along the A-B axis and appears to have a flatter spectrum than A or B, given its nondetection at 8 GHz. The detection of a third component along the continuum axis lends support to the idea that these represent features in a nuclear jet rather than, for instance, physically unconnected starburst regions. It appears that none of these three sources marks the nuclear engine of NGC 3079, which may be heavily absorbed. A more extended source (C) was detected at 22 GHz only; it may in fact be weak water maser emission that is amplifying undetected background continuum.

Water maser features in NGC 3079 trace a roughly north-to-south extended structure, consistent with the emission arising in a nearly edge-on disk aligned with the kiloparsec-scale molecular disk. The distribution of redshifted and blueshifted maser features is consistent with rotation in the same sense as the larger disk, with a binding mass on the order of $10^6\ M_\odot$. However, the velocity dispersion of clumps within the distribution and the suggestion of internal velocity gradients within the clumps indicate that nonrotational, possibly turbulent motions are significant. The masers may arise in shocks driven by a wide opening-angle nuclear wind. Two additional features were observed along the axis of the nuclear jet and may represent a second population of maser emission.

REFERENCES

Baan, W. A., & Haschick, A. D. 1996, ApJ, 473, 269
Baan, W. A., & Irwin, J. A. 1995, ApJ, 446, 602
Collison, A. J., & Watson, W. D. 1995, ApJ, 452, L103
Deguchi, S., & Watson, W. D. 1989, ApJ, 340, L17
Devereaux, N. 1987, ApJ, 323, 91
Diamond, P. J., Claussen, M. J., Braatz, J. A., Wilson, A. S., & Henkel, C. 1998, in IAU Colloq. 164, Radio Emission from Galactic and Extragalactic Compact Sources, ed. G. B. Taylor, J. M. Wrobel, & J. A. Zensus (San Francisco: ASP), in press
Dopita, M. A. 1995, Ap&SS, 233, 215
Duric, N., & Seaquist, E. R. 1988, ApJ, 326, 574
Elitzur, M. 1992, Astronomical Masers (Dordrecht: Kluwer)
Elitzur, M., Hollenbach, D. J., & McKee, C. F. 1989, ApJ, 346, 983
———. 1992, ApJ, 394, 221
Elitzur, M., McKee, C. F., & Hollenbach, D. J. 1991, ApJ, 367, 333
Elmegreen, B. G., & Morris, M. 1979, ApJ, 229, 593
Fabbiano, G., Feigelson, E., & Zamorani, G. 1982, ApJ, 256, 397
Filippenko, A. V., & Sargent, W. L. W. 1992, AJ, 103, 28
Ford, H. C., Dahari, O., Jacoby, G. H., Crane, P. C., & Ciardullo, R. 1986, ApJ, 311, L7
Gallimore, J. F., Baum, S. A., O'Dea, C. P., Brinks, E., & Pedlar, A. 1996, ApJ, 462, 740
Goldreich, P., & Keeley, D. A. 1972, ApJ, 174, 517
Greenhill, L. J. 1990, Ph.D. thesis, Harvard Univ.
Gwinn, C. R. 1994, ApJ, 429, 241
Gwinn, C. R., Moran, J. M., & Reid, M. J. 1992, ApJ, 393, 149
Hartquist, T. W., & Dyson, J. E. 1987, MNRAS, 228, 957
Haschick, A. D., & Baan, W. A. 1985, Nature, 314, 144
Haschick, A. D., Baan, W. A., Schneps, M. H., Reid, M. J., Moran, J. M., & Güsten, R. 1990, ApJ, 356, 149
Hawarden, T. G., Israel, F. P., Geballe, T. R., & Wade, R. 1995, MNRAS, 276, 1197
Hawarden, T. G., Mountain, C. M., Leggett, S. K., & Puxley, P. J. 1986, MNRAS, 221, 41P
Heckman, T. M. 1980, A&A, 87, 152
Heckman, T. M., Armus, L., & Miley, G. K. 1990, ApJS, 74, 833
Henkel, C., Guesten, R., Thum, C., & Downes, D. 1984, IAU Circ. 3983
Herrnstein, J. R. 1997, Ph.D. thesis, Harvard Univ.
Irwin, J. A., & Seaquist, E. R. 1988, ApJ, 335, 658
———. 1991, ApJ, 371, 111
Irwin, J. A., & Sofue, Y. 1992, ApJ, 396, L75
Kartje, J. F., Königl, A., & Elitzur, M. 1996, BAAS, 188, 4.02
Kaufman, M. J., & Neufeld, D. A. 1996, ApJ, 456, 250
Königl, A., & Kartje, J. F. 1994, ApJ, 434, 446
Melnick, G. J., Menten, K. M., Phillips, T. G., & Hunter, T. R. 1993, ApJ, 416, L37
Miyoshi, M., Moran, J. M., Herrnstein, J. R., Greenhill, L. J., Nakai, N., Diamond, P. J., & Inoue, M. 1995, Nature, 373, 127
Mac Low, M.-M., Elitzur, M., Stone, J. M., & Königl, A. 1994, ApJ, 427, 914
Nakai, N., Inoue, M., Miyazawa, K., Miyoshi, M., & Hall, P. 1995, PASJ, 47, 771
Neufeld, D. A., Maloney, P. R., & Conger, S. 1994, ApJ, 436, L127
Norman, C., & Silk, J. 1979, ApJ, 228, 197
O'Dea, C. P., Baum, S. A., & Stanghellini, C. 1991, ApJ, 380, 66
Pedlar, A., Mundell, C. G., Gallimore, J. F., Baum, S. A., & O'Dea, C. P. 1996, Vistas Astron., 40, 91
Phillips, R. B., & Mutel, R. L. 1982, A&A, 106, 21
Readhead, A. C. S., Taylor, G. B., Pearson, T. J., & Wilkinson, P. N. 1996, ApJ, 460, 634
Reid, M. J., & Moran, J. M. 1988, in Galactic and Extragalactic Radio Astronomy, ed. G. L. Verschuur & K. I. Kellermann (Berlin: Springer), 255
Satoh, S., Inoue, M., Nakai, N., Shibata, K. M., Kameno, S., Migenes, V., & Diamond, P. J. 1998, in IAU Colloq. 164, Radio Emission from Galactic and Extragalactic Compact Sources, ed. G. B. Taylor, J. M. Wrobel, & J. A. Zensus (San Francisco: ASP), in press
Sofue, Y., & Irwin, J. A. 1992, PASJ, 44, 353
Strel'nitskii, V. S., & Sunyaev, R. A. 1973, Soviet Astron., 16, 579
Tarter, T. C., & Welch, W. J. 1986, ApJ, 305, 467
Veilleux, S., Cecil, G., Bland-Hawthorn, J., Tully, R. B., Filippenko, A. V., & Sargent, W. L. W. 1994, ApJ, 433, 48
Wallin, B. K., & Watson, W. D. 1997, ApJ, 476, 685
Wardle, M. 1990, MNRAS, 246, 98
Young, J. S., Claussen, M. J., & Scoville, N. Z. 1988, ApJ, 324, 115

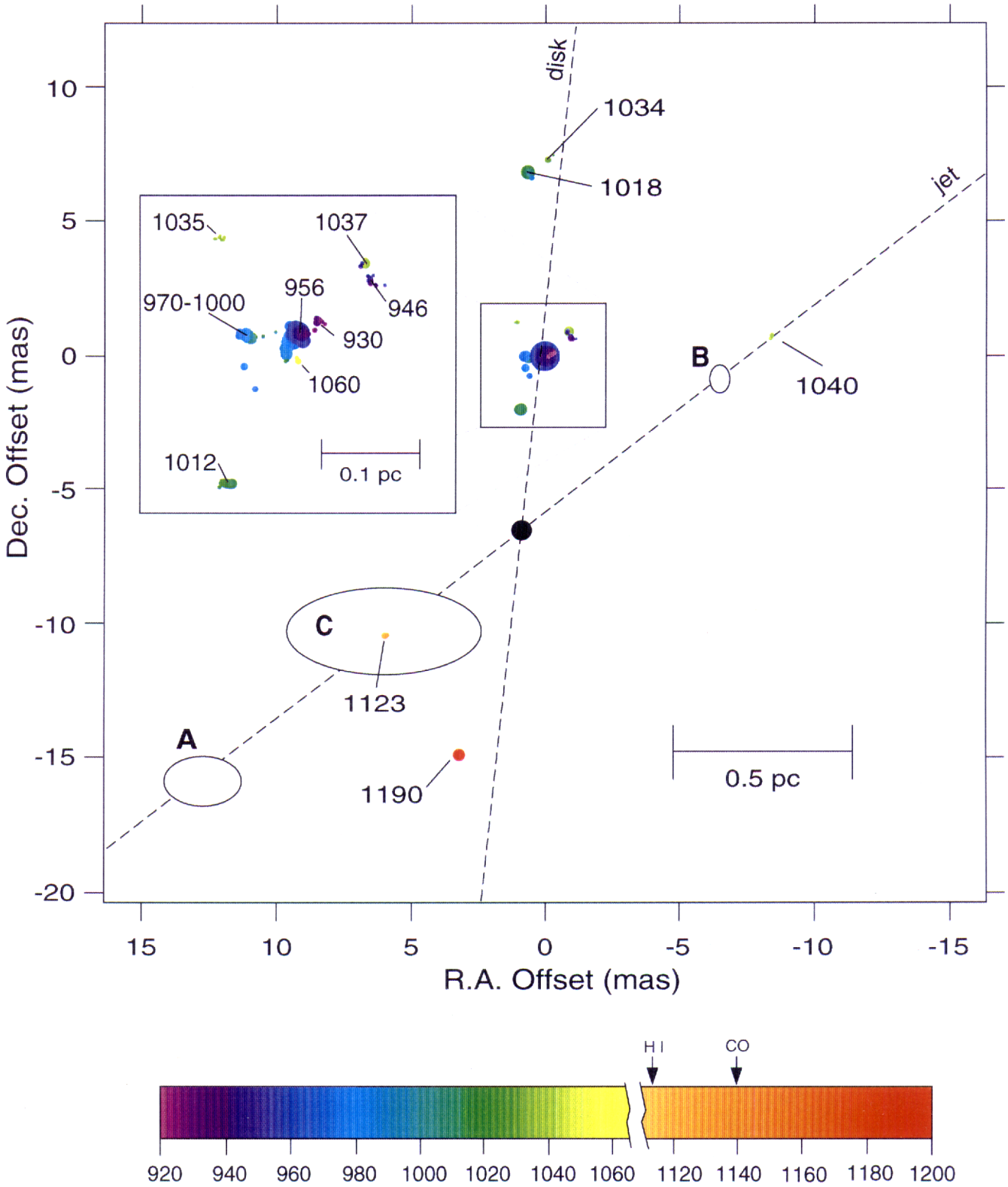

FIG. 1.—Map of the distribution of 22 GHz H_2O maser emission in the inner parsec of NGC 3079, observed with the VLBA in 1995 January. Colored circles mark the positions of maser features detected at the 5 σ level in 0.8 km s^{-1} wide spectral channel images. Color indicates the LSR Doppler velocity of the spectral channel; the scale is given by the color bar at the bottom of the image. The systemic velocities determined from H I and CO observations are marked with arrows. The approximate velocities of the peak emission in each clump are indicated on the map. The diameter of each circle is proportional to the logarithm of its flux density. The nearly vertical dashed line indicates the major axis of the kiloparsec-scale molecular disk. A second dashed line indicates the axis of the nuclear jet. The proposed position of the central engine is marked at the intersection of these two axes. Ovals indicate the positions and approximate angular sizes of the 22 GHz continuum features. The labels A, B, and C reflect the nomenclature of the 5 GHz VLBI image of Irwin & Seaquist (1988). *Inset*: Expanded view of the maser feature distribution within 0.1 pc of the maser peak, at the origin.

TROTTER et al. (see 495, 742)

PLATE 18